Development of Reluctance Actuator for High-Precision Positioning and Scanning Motion

1st Ines Burgstaller
Automation and Control Institute (ACIN)
TU Wien, Vienna, Austria
e1635278@student.tuwien.ac.at

2nd Shingo Ito
Christian Doppler Laboratory for Precision Engineering for Automated In-Line Metrology
Automation and Control Institute (ACIN)
TU Wien, Vienna, Austria
ito@acin.tuwien.ac.at

3rd Hiroshi Fujimoto
Department of Advanced Energy
Graduate School of Frontier Sciences
The University of Tokyo
Tokyo, Japan
fujimoto@k.u-tokyo.ac.jp

4th Georg Schitter
Christian Doppler Laboratory for Precision Engineering for Automated In-Line Metrology
Automation and Control Institute (ACIN)
TU Wien, Vienna, Austria
schitter@acin.tuwien.ac.at

2021 IEEE International Conference on Mechatronics (ICM) | 978-1-7281-4442-9/21/$31.00 ©2021 IEEE | DOI: 10.1109/ICM46511.2021.9385649

***Abstract*—To utilize the high force of reluctance actuators for high-precision fast scanning motion, this paper presents a nanopositioner that integrates two reluctance actuators for a bidirectional force and investigates its achievable performance. A challenge of reluctance actuators is their force-current nonlinearity. To model it accurately for compensation, a displacement sensor for real-time motion control is utilized to measure the force curves. A model based on the experiments is used to compensate for the nonlinearity by means of feedback linearization. It successfully decreases a total harmonic distortion of sinusoidal scanning trajectories from 25 % to 2.6 %, which is further improved to 1.45 % by linear position feedback control. The achieved bandwidth and the positioning resolution are 335 Hz and 2 nm. Additionally, feedforward control is designed, and sinusoidal scanning motions at 1 Hz and 100 Hz are evaluated for a feasibility study to find out challenges and potentials of reluctance actuators.**

***Index Terms*—high-precision actuators, nanopositioning, reluctance actuator, feedback linearization**

I. Introduction

High-precision, high-frequency scanning motion is important for high performance systems, such as optical scanners [1], nanopositioners for atomic force microscopes [2] and wafer scanners [3]. In such systems, Lorentz actuators are a most commonly used short-stroke electromagnetic actuator.

Lorentz actuators utilize the Lorentz force, which shows high linearity between the coil current and the resulting force that is almost independent of the mover position [4]. This is beneficial for control design to generate highly precise motion [5]. However, they have a low motor constant, which is the force-to-current ratio. As a result, a large current is necessary for a high force to accelerate the mover, heating up the coil. Thus, the energy is wasted and a cooling system is often necessary [4].

One of the promising actuators for scanning motion is reluctance actuators because they exhibit higher force density (force per mass) and generate lower heat than Lorentz actuators [4], [6]. For these advantages, reluctance actuators are widely used for magnetic bearings that suspend a mover (e.g. a rotor or shaft) in the air [7]–[9], where disturbance rejection performance is important to position the mover at a static point [10], rather than the reference tracking performance for scanning motion. A concern of reluctance actuators is nonlinearities, such as eddy currents, magnetic hysteresis, and the nonlinear relation between the coil current and the force that depends on the mover position [3].

For high-precision scanning motion, reluctance actuators' nonlinearities have to be compensated. Nonlinearities such as eddy currents and magnetic hysteresis can be reduced to some extent by manufacturing the stator and the mover from laminated layers of a soft ferromagnetic material [11]. To compensate for the force-current nonlinearity, it is often investigated by force sensors [12], [13]. However, there are a few concerns. For example, mounting a force sensor is simply difficult when the actuator is compact (cf. [14]). Installing a force sensor may create a crosstalk such as a torque, depending on the mounting location and the assembly precision. Furthermore, some force sensors themselves can have inherent nonlinearities [15], [16], which are inappropriate to accurately evaluate the actuator nonlinearity. Therefore, it is desired to evaluate the force-current nonlinearity by using the internal displacement sensor for real-time control.

This paper proposes a nanopositioner based on reluctance actuators and investigates their capability to realize a high-frequency scanning motion with nanometer resolution. The

978-1-7281-4442-9/21/$31.00 ©2021 IEEE

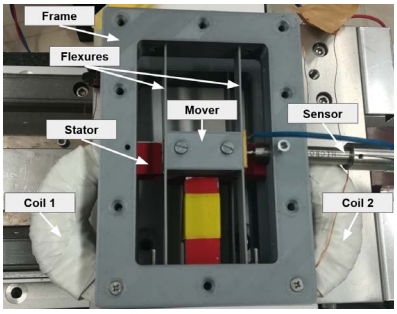

(a) Photograph of the nanopositioner.

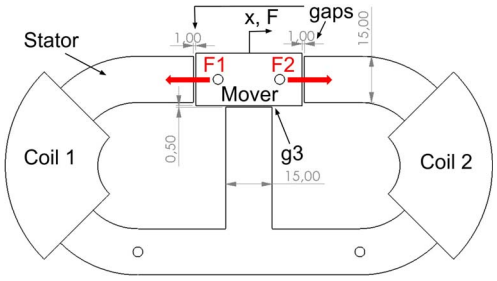

(b) Illustration of the reluctance actuator without frames and flexures.

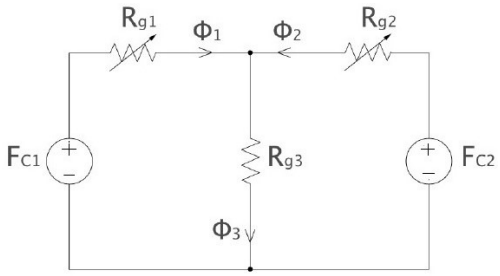

(c) Magnetic circuit of the actuator.

Fig. 1: Proposed double variable reluctance actuator (dimensions in mm).

nanopositioner uses a capacitive displacement sensor for feedback control and a pair of reluctance actuators for high-frequency bidirectional scanning motion (i.e. double variable reluctance actuator). The force-current nonlinearity of the reluctance actuators is investigated by using the capacitive displacement sensor without a force sensor. The results are used to derive a nonlinear model for compensation with feedback linearization. For the linearized system, linear feedback and feedforward control are designed. Experiments are carried out to demonstrate scanning motions with nanometer resolution and to identify potential challenges.

II. System Description

Fig. 1(a) shows a photograph of the proposed nanopositioner. It consists of an E-shaped stator, a mover and two identical coils. To reduce eddy current losses the stator and mover are manufactured from ferromagnetic laminated steel sheets. The mover is laterally guided with a designed range of 2 mm by 3D printed frames that include flexures. The mover position is measured by a capacitive displacement sensor (6810, Microsense, Hamm, Germany), which has a nominal resolution and linearity of 1 nm and 0.25 %, respectively. The coils are individually driven by current amplifiers to provide a maximum current of 2 A. The bandwidth of the amplifiers is 6.5 kHz. Control algorithms are implemented by a rapid control prototyping system (DS1005, dSpace, Paderborn, Germany) with a sampling frequency of 20 kHz which is connected to the current amplifiers with 16-Bit DACs.

III. Actuator Model

Fig. 1(c) illustrates the magnetic circuit of the nanopositioner. The reluctances of the air gaps are modelled as $\mathcal{R}_{g1}$, $\mathcal{R}_{g2}$ and $\mathcal{R}_{g3}$. The magnetomotive forces F_{C1} and F_{C2} are generated by the two coils, and the magnetic fluxes through the three air gaps are denoted by Φ_1, Φ_2 and Φ_3, respectively. Due to the high permeability of the ferromagnetic parts, their reluctance is sufficiently smaller than that of the air gaps and is thus neglected. The reluctances of the air gaps are

$$\mathcal{R}_{g1} = \frac{g+x}{\mu_0 A}, \mathcal{R}_{g2} = \frac{g-x}{\mu_0 A}, \mathcal{R}_{g3} = \frac{g_3}{\mu_0 A}, \tag{1}$$

where $g = 1$ mm is the variable air gaps for a maximum motion of $\pm$ 1 mm when the mover is in its center position, g_3 is the fixed air gap of 0.5 mm, x is the position of the mover (Fig. 1(b)), and μ_0 and A are the permeability of vacuum and the cross-sectional area of the actuator, respectively. By applying Hopkinson's law [17], and the superposition principle of linear circuits with the number of coil turns N and the coil currents I_1 and I_2, the fluxes through the variable air gaps Φ_1 and Φ_2 are calculated.

The forces acting on both sides of the mover (F_1, F_2) along the actuation axis can be derived by applying Maxwell's stress tensor [18] and are given by

$$F_1 = \frac{\Phi_1^2}{2\mu_0 A}, F_2 = \frac{\Phi_2^2}{2\mu_0 A}. \tag{2}$$

The total reluctance force F_R acting on the mover is obtained from those forces and simplified as follows

$$F_R = F_2 - F_1 = -\frac{A\mu_0 N^2 (I_1^2 - I_2^2)}{2g(g+2g_3)}, \tag{3}$$

when the mover is in its center position $x = 0$. Notice the nonlinearity due to the squared currents and g in the denominator.

IV. Feedback Linearization

To handle the force-current relationship, feedback linearization [7] and gain scheduling [19] are often employed. In gain scheduling, the nonlinearity is linearized at different operating points and different controllers are designed for each operating point. A disadvantage is that the range must be split into fine intervals to achieve high-resolution results, resulting in large lookup tables of the controller gains [20]. In feedback linearization a nonlinear plant is linearized by using an inverted nonlinear model in series in front of the plant for compensation [13]. Feedback linearization can significantly increase the linearity over an extended range [10], which is necessary for high-precision scanning motion. Thus feedback linearization is implemented in this paper.

The block diagram for the nanopositioner is shown in Fig. 2. To position the mover, the coils are switched instead of providing a constant bias current to increase the energy efficiency. First, to linearize the actuator, the force-current nonlinearity

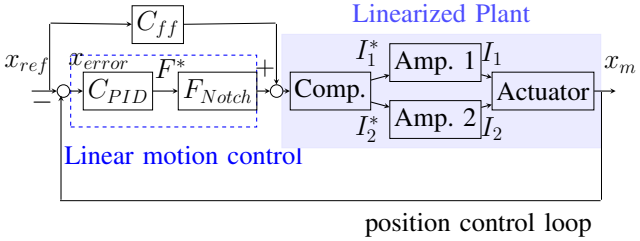

Fig. 2: Control block diagram of the nanopositioner.

is compensated by feedback linearization, which is denoted by the "Comp." block. Then linear motion control is applied for precision motion. To improve the scanning performance, an additional inversion based feedforward control (C_{ff}) is implemented for the experiments.

A. Force Profile Measurement

As a feasibility study of a nanopositioner based on reluctance actuators, a model of their force-current nonlinearity is experimentally created under an assumption that the mover motion is sufficiently small around the origin $x = 0$. This is because the analytical model (Eq. (3)) does not account for fringing and leakage flux as well as assembly and manufacturing tolerances that degrade the model accuracy, which is problematic for feedback linearization.

The forces F_1 and F_2 on both sides of the mover are given as functions of the respective coil currents I_1 and I_2 as follows

$$F_1 = f_1(I_1), F_2 = f_2(I_2). \tag{4}$$

As the first step, the motor constant curve of Coil 1 is measured. For this purpose, DC currents I_{DC1} and I_{DC2} are applied to Coil 1 and Coil 2, respectively, such that the mover stays around the equilibrium point at $x = 0$. Then, an additional sine current is superimposed to Coil 1 at a frequency sufficiently higher than the natural frequency of the flexure-suspended mover, where its mass $m = 1\,\text{kg}$ dominates the dynamics as follows

$$F_R(s) = F_2 - F_1 = m \cdot s^2 \cdot \Delta x(s), \tag{5}$$

with the Laplace variable s and the deviation of the mover from its center position Δx. By applying a first-order Taylor expansion around the mover position $x = 0$ and the DC current levels I_{DC1} the reluctance force F_R is approximated considering that at x = 0 the forces on both sides of the mover are balanced $f_1(I_{DC1}) = f_2(I_{DC2})$, as follows

$$\begin{aligned} F_R &\approx f_2(I_{DC2}) - (f_1(I_{DC1}) + \frac{\partial f_1}{\partial I}\Big|_{I=I_{DC1}} \cdot \Delta I_{AC}) \\ &= -\frac{\partial f_1}{\partial I}\Big|_{I=I_{DC1}} \cdot \Delta I_{AC}, \end{aligned} \tag{6}$$

with ΔI_{AC} being the distance of the measured current of Coil 1 to the operating points I_{DC1} that occurs due to the superposition of the sinusoidal current to Coil 1. The motor constant K_{m1} is regarded as the change in the force due to a change in the current, thus it is given by

$$K_{m1} = \frac{\partial f_1}{\partial I}\Big|_{I=I_{DC1}}. \tag{7}$$

Eq. (5)-(7) imply that the motor constant at a DC current can be calculated by measuring the amplitude of the sinusoidal current and the resulting mover oscillation.

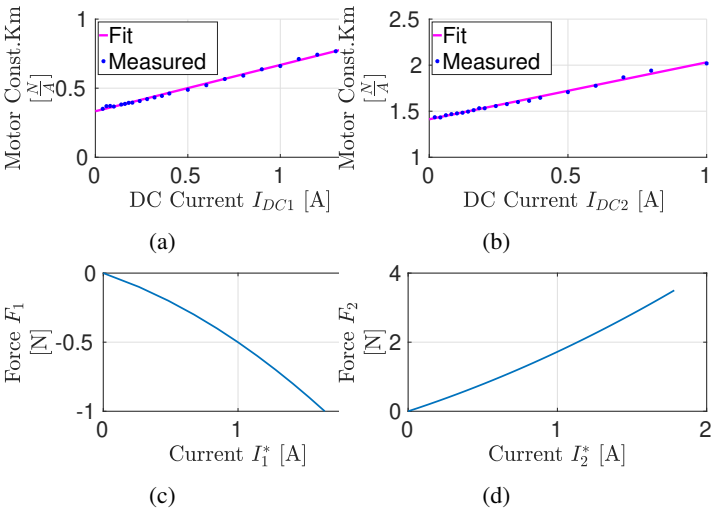

Fig. 3: Reconstructed motor constant (a),(b) and force curve (c),(d) for both coils.

B. Model-based Linearization

To measure the motor constant-current curve, a current with a frequency of 100 Hz and a small peak-to-peak amplitude of $40\,mA_{pp}$ is applied to the system and the DC current levels (I_{DC1}, I_{DC2}) are varied over a range from 0 A to 1.5 A to keep the mover in its center position, while evaluating different current levels. The data points are measured from 0 A to around 1.5 A and then in the same manner for Coil 2 to prevent an error due to hysteresis. The measurements can be seen in Fig. 3(a) for Coil 1 and 3(b) for Coil 2. Due to the small amplitudes of the current and position signal, which are caused by superimposing the sine wave to the DC current, there is a small offset in both curves. To the measured data points, linear equations are fitted and integrated over the current range to obtain the force-current curve, as shown in Fig. 3(c)-(d). Due to manufacturing tolerances and assembly precision those curves are not symmetric, limiting the effective force and movement range. To linearize this relationship, the obtained force-current curves for both coils are inverted, to calculate the desired current I to reach the desired reluctance force F, as follows

$$I = \begin{cases} -1 \pm 0.3 \cdot 10^{-3}\sqrt{1.1 \cdot 10^7 - 6.7 \cdot 10^7 \cdot F}, & F < 0 \\ -2.3 \pm 0.8 \cdot 10^{-3}\sqrt{7.98 \cdot 10^6 + 4.9 \cdot 10^6 \cdot F}, & F > 0. \end{cases} \tag{8}$$

The switching between the coils happens when the desired force reaches zero. This calculation is implemented on the rapid control prototyping system.

C. Validation

To evaluate the nonlinearity without compensation, a sine current reference is applied to the system with a frequency of 1 Hz and an amplitude of 0.5 A. The mover position and current reference are recorded by the rapid control prototyping system, as shown in Fig. 4(a). There are distortions in the

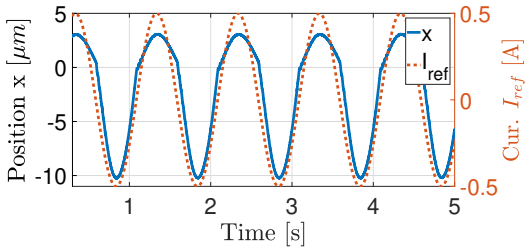

(a)

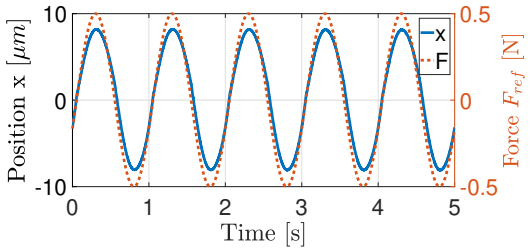

(b)

Fig. 4: Recorded position signal without (a) and with linearization (b) for a reference signal with a freqency of 1 Hz.

measured position signal. To evaluate the nonlinearity, the total harmonic distortion (THD) of the position signal is calculated. It represents the harmonic components of a signal compared to its fundamental frequency [21]. The THD of the position sine wave is calculated with the fundamental frequency and the first five harmonics, which are the dominant harmonics in the signal. The THD of the measured sensor signal is 25 %.

When the feedback linearization is used, a sine reference force with a frequency of 1 Hz and an amplitude of 0.5 N is applied, and the mover position and force reference are recorded, as shown in Fig. 4(b). The position signal shows a smooth sine wave without major distortions. The THD is successfully reduced from 25 % to 2.56 % by applying the feedback linearization.

D. Frequency Response

A frequency response of the linearized plant is measured by a network analyzer (3562A, HP, Palo Alto, USA) from the force reference to the mover position by applying a sine sweep from 1 Hz to 5 kHz with an amplitude of 50 mV_{pp}. The frequency response in Fig. 5 is evaluated at different mover positions in a range of 50 μm, by applying an offset to the applied reference signal. The magnitude line in Fig. 5 shows a variation up to 30 % between different mover positions. This

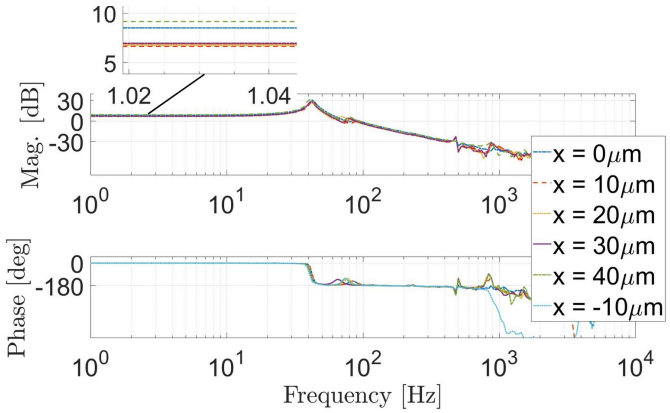

Fig. 5: Bode plot of the linearized plant from the reference force to the output position at different mover positions.

is due to residual nonlinearity in the system, such as magnetic hysteresis.

V. Motion Control

To reject disturbances for precision motion, a feedback controller is designed for the linearized actuator (Fig. 2). To suppress the bandwidth-limiting resonance at 480.6 Hz (see Fig. 5) that is insensitive to the mover position, a notch filter F_{Notch} is designed as follows

$$F_{Notch}(s) = \frac{s^2 + 0.1 \cdot \omega_{N,1} \cdot d_n \cdot s + \omega_{N,1}^2}{s^2 + 0.1 \cdot \omega_{N,1} \cdot s + \omega_{N,1}^2}, \tag{9}$$

with the notch frequency $\omega_{N,1} = 2\pi \cdot 480.6 \ \frac{rad}{s}$ and the depth of the notch $d_n = 0.07$, which is calculated from the height of the resonance peak [22]. This notch filter is placed in series with a tamed PID controller C_{PID} [3] to provide with sufficient phase lead around the desired open-loop crossover frequency ω_C and eliminate the steady-state error. It is given by

$$C_{PID}(s) = k_p + \frac{k_i}{s} + \frac{k_d \cdot s}{1 + \frac{s}{\omega_t}}. \tag{10}$$

The controller gains are tuned to

$$k_p = 2.56, k_i = 358.87, k_d = 28.42, \omega_t = 4.68 \cdot 10^3, \tag{11}$$

to maximize ω_C with sufficient stability margin. The achieved gain margin is over 9 dB, and the achieved phase margin is over 47 ° for all evaluated mover positions in a range of 60 μm. The maximised ω_C is 180 Hz.

Fig. 6 shows the measured complementary sensitivity function for different mover positions in a range of 60 μm for validation. The achieved closed-loop bandwidth is 335 Hz.

VI. Experiments and Results

A. Evaluation of the Closed-Loop Linearity

The linearity with the feedback control is evaluated. A reference position signal with a frequency of 1 Hz and an amplitude of 10 μm is applied, and the mover position and

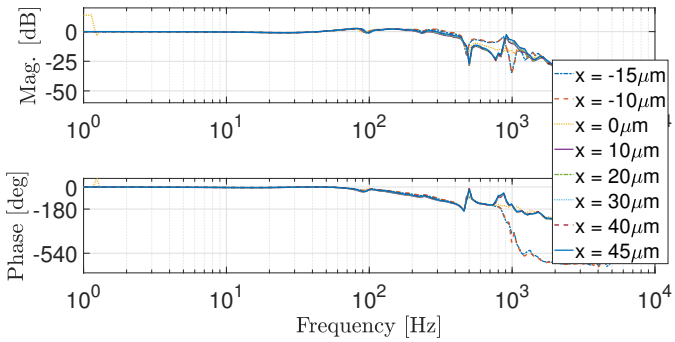

Fig. 6: Measured complementary sensitivity function at different mover positions.

reference are recorded and shown in Fig. 7. By applying feedback control, the THD is further reduced to 1.45 %.

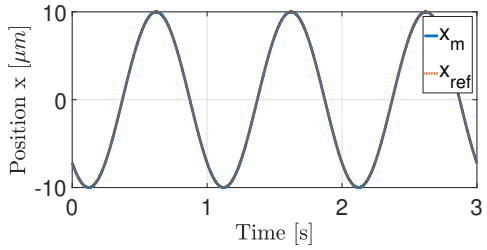

Fig. 7: Reference position signal with an amplitude of 10 μm and a frequency of 1 Hz and recorded position signal.

B. Positioning Resolution and Step Response

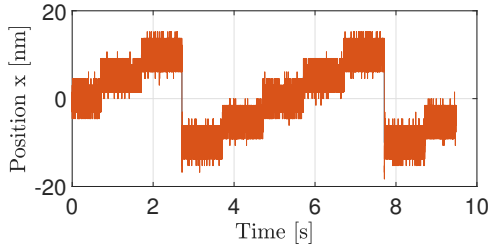

Fig. 8: Measured step with a height of 5 nm, symmetric around the position $x = 0\,\mu m$.

The positioning resolution of the nanopositioner is evaluated at static points when the feedback control is activated. Fig. 8 clearly shows that the positioning resolution is 7 nm and 2 nm when it is evaluated by a peak-to-peak and RMS value, respectively. Consequently 5 nm steps are clearly resolved in Fig. 8. Note that the quantization noise is 1.5 nm due to the ADC resolution. Overall, this experiment demonstrates the capability of reluctance actuators for nanometer-resolution positioning.

C. Scanning Motion

To evaluate scanning motion, a plant model $P(s)$ is created based on the frequency response in Fig. 5, then inverted as a feedforward controller $C_{ff}(s)$ in Fig. 2 and combined with a second order low-pass filter with a cutoff frequency of 400 Hz, above which the model uncertainty increases. The detailed design of C_{ff} is not shown in this paper.

To evaluate fast scanning with a small amplitude, a reference position with an amplitude of 2.5 μm and a frequency of 100 Hz is applied to the actuator. The recorded reference and measured position are shown in Fig. 9(d), the corresponding coil currents are shown in Fig. 9(e) and the error between the reference and measured position is shown in Fig. 9(f). As is visible in the error signal (Fig. 9(f)), it is smooth, showing the nanopositioner's capability to realize fast smooth scanning trajectories. The error has a frequency of 100 Hz, an amplitude of $\pm$ 420 nm, which corresponds to 16.8 % of the reference amplitude and a RMS error of 295 nm. This error is large compared to the previously evaluated static positioning error and may be reduced by applying advanced control, such as learning control [22], [23].

To evaluate slow scanning over a long range, a sine reference position signal with a frequency of 1 Hz and an amplitude of 15 μm is applied. The recorded reference and measured

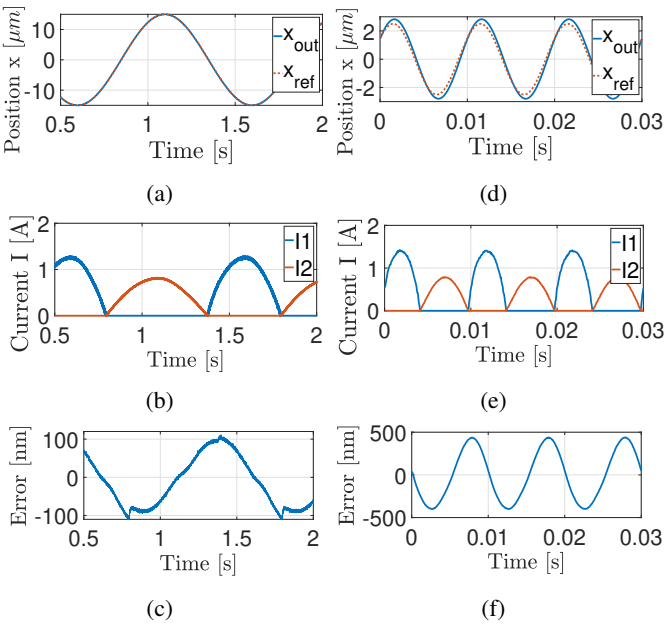

Fig. 9: Position reference and measured position, Coil currents and error for a reference signal with an amplitude of 15 μm and a frequency of 1 Hz (a-c) and with an amplitude of 2.5 μm and a frequency of 100 Hz (d-f).

position signals are shown in Fig. 9(a), the corresponding coil currents are shown in Fig. 9(b) and the error between reference and measured position is shown in Fig. 9(c). The error shows an amplitude of $\pm$100 nm, which corresponds to 0.67 % of the

amplitude of the reference signal and a RMS error of 66.3 nm.

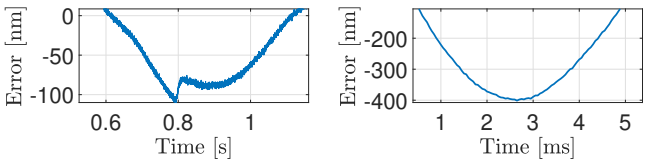

(a) (b)

Fig. 10: Magnified error signals for a 1 Hz reference (a) and a 100 Hz reference (b) at coil switching points.

Fig. 9(c) shows jumps that are introduced into the error signal at low frequency sine scanning motion by switching between the coils. They have a maximum height of 25 nm, which corresponds to 0.17 % of the reference amplitude. The error signals from Fig. 9(c) and (f) are magnified at the switching points in Fig. 10(a) for 1 Hz and 10(b) for 100 Hz, where the current switching points occur at 0.8 s and 4 ms for 1 Hz and 100 Hz respectively. The jumping that is visible at the switching point of the 1 Hz signal is not observable for high frequency scanning motion above 10 Hz as shown in Fig. 10(b). Therefore it is assumed that those jumps are due to rate-dependent effects, such as the hysteresis.

In summary the experiments successfully demonstrate the capability of the reluctance actuators to realize a single nanometer positioning resolution and smooth fast scanning motion, while they identify the coil switching as a challenge of long range slow scanning.

VII. Conclusion

This paper proposes a nanopositioner based on reluctance actuators to evaluate its performance in positioning and scanning with nanometer resolution. The capacitive displacement sensor for real time control is utilized to accurately model the nonlinear force-current relation. The result is used for feedback linearization, successfully decreasing the THD of a sine scanning motion from 25 % to 2.56 % and further to 1.45 % by applying feedback control that achieves a closed-loop bandwidth of 335 Hz and a positioning resolution of 2 nm for a range of 60 μm. While the nanopositioner with additional feedforward control enables a smooth motion at a high scanning frequency of 100 Hz, a jumping motion due to the coil current switch is identified as a potential challenge for slow scanning motion. Future work includes further analysis of the rate dependent nonlinearity and its compensation by applying advanced motion control.

Acknowledgment

The financial support by the Christian Doppler Research Association, the Austrian Federal Ministry for Digital and Economic Affairs, the National Foundation for Research, Technology and Development, MICRO-EPSILON MESSTECHNIK GmbH & Co. KG and ATENSOR Engineering and Technology Systems GmbH, and the JASEC is gratefully acknowledged.

References

[1] S. Ito, M. Poik, E. Csencsics, J. Schlarp, and G. Schitter, "High-speed scanning chromatic confocal sensor for 3-d imaging with modeling-free learning control," *Appl. Opt*, vol. 95, no. 29, pp. 9234–9242, 2020.

[2] P. Eaton and P. West, *Atomic force microscopy*. Oxford university press, 2010.

[3] R. M. Schmidt, G. Schitter, A. Rankers, and J. Eijk, *The Design of High Performance Mechatronics*, 3rd ed. IOS Press BV, Amsterdam, 2020.

[4] N. Vrijsen, J. Jansen, and E. Lomonova, "Comparison of linear voice coil and reluctance actuators for high-precision applications," in *Proceedings of IEEE International Power Electronics and Motion Control Conference*, 2010, pp. S3–29.

[5] X. Feng, Z. Duan, Y. Fu, A. Sun, and D. Zhang, "The technology and application of voice coil actuator," in *IEEE Second International Conference on Mechanic Automation and Control Engineering*, 2011, pp. 892–895.

[6] A. Katalenic, H. Butler, and P. P. van den Bosch, "High-precision force control of short-stroke reluctance actuators with an air gap observer," *IEEE/ASME Transactions on Mechatronics*, vol. 21, no. 5, pp. 2431–2439, 2016.

[7] M. Chen and C. R. Knospe, "Feedback linearization of active magnetic bearings: current-mode implementation," *IEEE/ASME Transactions on Mechatronics*, vol. 10, no. 6, pp. 632–639, 2005.

[8] J. D. Lindlau and C. R. Knospe, "Feedback linearization of an active magnetic bearing with voltage control," *IEEE Transactions on control systems technology*, vol. 10, no. 1, pp. 21–31, 2002.

[9] G. Schweitzer, E. H. Maslen *et al.*, *Magnetic bearings: theory, design, and application to rotating machinery*. Springer Berlin, 2009, vol. 1.

[10] A. Katalenic, "Control of reluctance actuators for high-precision positioning," Ph.D. dissertation, Eindhoven University of Technology, 2013.

[11] A. Katalenic, J. De Boeij, H. Butler, and P. Van Den Bosch, "Linearization of a current-driven reluctance actuator with hysteresis compensation," *Mechatronics*, vol. 23, no. 2, pp. 163–171, 2013.

[12] S. Roux, F. M. Carter, and R. I. Mackenzie, "Method for controlling the position of a movable object, a control system for controlling a positioning device, and a lithographic apparatus," Oct. 8 2013, uS Patent 8,553,205.

[13] I. R. I. MacKenzie, "Design and control methods for high-accuracy variable reluctance actuators," Ph.D. dissertation, Massachusetts Institute of Technology, 2015.

[14] S. Ito, F. Cigarini, and G. Schitter, "Flux-controlled hybrid reluctance actuator for high-precision scanning motion," *IEEE Transactions on Industrial Electronics*, vol. 67, no. 11, pp. 9593–9600, 2020.

[15] J.-S. Kim and G.-W. Kim, "Hysteresis compensation of piezoresistive carbon nanotube/polydimethylsiloxane composite-based force sensors," vol. 17, no. 2. Multidisciplinary Digital Publishing Institute, 2017, p. 229.

[16] X. Shi, C.-H. Cheng, Y. Zheng, and P. Wai, "An egain-based flexible piezoresistive shear and normal force sensor with hysteresis analysis in normal force direction," *Journal of Micromechanics and Microengineering*, vol. 26, no. 10, p. 105020, 2016.

[17] H. Frohne, K.-H. Löcherer, H. Müller, and F. Moeller, *Moeller Grundlagen der Elektrotechnik*. Springer-Verlag, 2005.

[18] D. Wu, X. Xie, and S. Zhou, "Design of a normal stress electromagnetic fast linear actuator," *IEEE Transactions on Magnetics*, vol. 46, no. 4, pp. 1007–1014, 2009.

[19] Y.-C. Kim, S.-K. Ryu *et al.*, "Gain scheduled control of magnetic suspension system," *Control Robotics Society: Conference Papers*, pp. 321–326, 1993.

[20] D. L. Trumper, S. M. Olson, and P. K. Subrahmanyan, "Linearizing control of magnetic suspension systems," *IEEE Transactions on control systems technology*, vol. 5, no. 4, pp. 427–438, 1997.

[21] D. Shmilovitz, "On the definition of total harmonic distortion and its effect on measurement interpretation," *IEEE Transactions on Power delivery*, vol. 20, no. 1, pp. 526–528, 2005.

[22] S. Ito, S. Troppmair, B. Lindner, F. Cigarini, and G. Schitter, "Long-range fast nanopositioner using nonlinearities of hybrid reluctance actuator for energy efficiency," *IEEE Transactions on Industrial Electronics*, vol. 66, no. 4, pp. 3051–3059, 2019.

[23] H. Fujimoto and T. Takemura, "High-precision control of ball-screw-driven stage based on repetitive control using n-times learning filter," *IEEE Transactions on Industrial Electronics*, vol. 61, no. 7, pp. 3694–3703, 2014.